Layer-by-layer fabrication of highly transparent polymer based piezoelectric transducers

V. F. Cardoso[1,2,*], T. Marques-Almeida[1], T. Rodrigues-Marinho[1], G. Minas[2], L. Rebouta[1] and S. Lanceros-Mendez[3,4]

[1]Centro/Departamento de Física, Universidade do Minho, Campus de Gualtar, 4710-057 Braga, Portugal
[2]CMEMS-UMinho, Universidade do Minho, DEI, Campus de Azurém, Guimarães 4800-058, Portugal
[3]BCMaterials, Basque Center for Materials, Applications and Nanostructures, UPV/EHU Science Park, 48940 Leioa, Spain
[4]IKERBASQUE, Basque Foundation for Science, 48013-Bilbao, Spain

[*]E-mail: vanessa@dei.uminho.pt

Abstract. The fabrication of highly transparent piezoelectric transducers is of increasing interest in the scientific and technological community. In this work, polymer based piezoelectric transducers were fabricated by the direct deposition of each layer forming the transducer on the desired substrate, avoiding the use of coupling layers. Transparent conductive oxide (TCO) electrodes were deposited by magnetron sputtering and piezoelectric films based on the copolymer poly(vinylidene fluoride-*co*-trifluoroethylene) (P(VDF-TrFE)) were deposited by spin-coating. All layers were processed and characterized to obtain a highly transparent piezoelectric P(VDF-TrFE) transducer with a strong adhesion between layers and preserving the piezoelectric response of the copolymer film. Indium tin oxide (ITO), gallium-doped zinc oxide (GZO) and aluminium-doped zinc oxide (AZO) were evaluated, and the best performance was obtained with AZO. The optimized transducer features an optical transmittance higher than 75 % in the visible spectral range and a piezoelectric coefficient $|d_{33}|$ of 34 $pC.N^{-1}$.

Keywords: Piezoelectric, transducer, poly(vinylidene fluoride-*co*-trifluoroethylene), transparent conductive oxides, adhesion, transparency.

1. Introduction

In the last decades, polymers are increasingly replacing traditional materials in many technological fields, including electronics, automobile, aerospace and biomedical applications, among others. This phenomenon is related to the advantages of polymer materials that can be summarized by their flexibility, lightness, robustness, and low cost[1]. Thanks to the strong technological advances in this area, polymer based smart materials, capable of responding to external stimuli through a quantifiable and reproducible variation of at least one of their physicochemical characteristics, are increasingly integrated into advanced applications. Examples of stimuli are mechanical stress, temperature or pH change, electric or magnetic fields, among others[2-4]. Materials with the ability to convert electrical stimuli into a mechanical response, and vice versa, have acquired a significant relevance in the field of sensors and actuators and are mostly based on the piezoelectric effect[5-8]. The most relevant piezoelectric polymers are poly(vinylidene fluoride) (PVDF) and their copolymers such as poly(vinylidene fluoride-*co*-trifluoroethylene) (P(VDF-TrFE))[9]. The scientific and technological interest on piezoelectric polymers relies in the fact that they combine the characteristics of a plastic, such as mechanical and chemical resistance, flexibility and processability in different shapes, with those of a piezoelectric material. Further, these piezoelectric polymers are highly resistant to chemicals and aging[9, 10]. All these properties give them some advantages compared to piezoelectric ceramic. While ceramics are rigid and brittle, piezoelectric polymers are flexible and easily produced in the form of films or specific shapes, as previously stated. Moreover, when properly processed, these materials can show high optical transmittance in the visible spectral range, increasing their range of applications[11, 12].

To work as transparent piezoelectric transducer, the electrodes on both surfaces of the piezoelectric film should, also, show a high transmittance in the visible spectral range. The most commonly used piezoelectric transducers have metal electrodes, which make them opaque to light and difficult transmittances detection in optical systems. It is possible to find some piezoelectric transparent transducers in the literature for application as speakers or loudspeakers[13], touch screens[14] ultrasonic-optical systems for particle manipulation[15], and ultrasonic actuators[16], among others. The addition of optically transparent electrodes, such as poly(3,4-ethylenedioxythiophene) polystyrene sulfonate (PEDOT:PSS)[17, 18] or transparent conductive oxides (TOCs)[19, 20], allows the development of systems capable of detecting optoacoustic profiles in optoelectronic applications, such as biological systems for detection of penetration of transcutaneous medication. TCOs exhibit a high optical transmittance in the visible spectral range along with a high electrical conductivity[21, 22]. These materials are composed of oxides from metals such as indium, cadmium, tin and zinc[22]. Due to the application potential of these materials, TCO's have been the subject of intense studies, as shown by the large number of scientific papers and reviews published in this area[23-26]. Indium tin oxide (ITO) is nowadays the best known and studied TCO[27, 28], being applied in applications such as solar cells[29], liquid crystal displays (LCDs)[30], e-papers[31], touch panels[32] and light emitting diodes (LEDs)[33, 34]. However, the scarcity, high price and toxicity of indium encouraged the scientific community to find possible substitutes[35, 36]. Promising alternatives are aluminium-doped zinc oxide (AZO) and gallium-doped zinc oxide (GZO). Of these two, the best candidate is AZO since it is abundant in nature, low cost, non-toxic and present electrical resistivity comparable to ITO[37]. However, the choice of the material is not limited to these factors, being also dependent on the application requirements[38]. In fact, when developing piezoelectric PVDF based transducers, one of the precautions to take is

the temperature at which the electrodes are deposited that should be low (<80 ºC) in order to avoid the polymer overheating, which can compromise its integrity and piezoelectricity[39]. Moreover, a high adhesion between the electrodes and the piezoelectric polymer film should be guaranteed. In this work, the fabrication of highly transparent piezoelectric P(VDF-TrFE) transducers is presented (Figure 1).

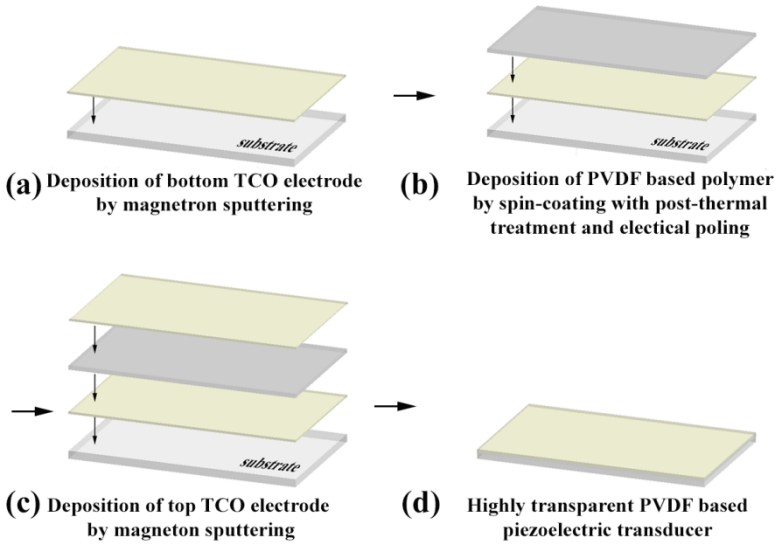

Figure 1: Schematic representation of the processing step to obtain highly transparent PVDF based piezoelectric transducers.

First, different TCO thin films, including ITO, AZO and GZO, were deposited in a glass substrate by magnetron sputtering. The P(VDF-TrFE) films were deposited by spin-coating, immediately submitted to a heat treatment and then poled by corona discharge. Spin-coating technique is widely used for the highly reproducible manufacture of films in large areas and with structural uniformity, an essential requirement for electromechanical applications. Moreover, this technique allows the deposition of films with a wide range of controllable thicknesses, from few nanometers to tens of micrometers[11, 12, 40]. Further, the direct deposition of films on the desired substrate prevent using coupling layers (such as glue and adhesive tape), which may reduce the transducer

efficiency. Finally, after poling of the P(VDF-TrFE) films, top TCO electrodes were deposited also by magnetron sputtering. All layers constituting the P(VDF-TrFE) transducer were processed and characterized to obtain a highly transparent system with a strong adhesion between layers and safeguarding the piezoelectricity of the copolymer film.

2. Materials and experimental methods

2.1. Materials

Indium tin oxide (In_2O_3/SnO_2 90/10 wt%) and zinc oxide doped with gallium oxide (ZnO/Ga_2O_3 95/05 wt%) sputtering targets, both with a diameter of 5 cm, were purchased from Kurt J. Lesker. Zinc oxide/aluminium oxide (98:2 wt%) sputtering target with a diameter of 10 cm was obtained from Gfe. P(VDF-TrFE), 70/30 (70 mol% vinylidene fluoride monomer; 30 mol% trifluoroethylene) powder was purchased from Solvay. Dimethylformamide (DMF) was supplied form Sigma Aldrich. All chemicals and solvents were used as received without further purification.

2.2. Experimental procedures

2.2.1. Deposition of the bottom TCO-based electrodes

Thin films of ITO, AZO and GZO were deposited by magnetron sputtering on highly polished and cleaned glass substrates with a thickness of 1 mm and an area of 40×24 mm^2. The introduction of gases into the chamber is carried out by two flow controllers (Bronkhorst HIT-TEC), with a maximum flow of 500 sccm for argon and 50 sccm for oxygen. Furthermore, the substrate holder within the deposition chamber allows a rotational movement and it is located at a distance of 8 cm from the target. The deposition

parameters, obtained after an optimization procedure to achieve TCO's thin films with good transparency and low resistivity, are indicated in Table 1. Nine samples were prepared for each TCO thin film.

Table 1: Deposition parameters of ITO, AZO and GZO thin films by magnetron sputtering.

Deposition parameters	ITO	AZO	GZO
Target current density (mA/cm^2)	2.6	2.5	5.1
Substrate bias (V)	-30	-28	-30
Frequency (kHz)	140	DC	DC
Duty cycle	0.7	-	-
Base pressure (Pa)	2.9×10^{-4}	2×10^{-4}	2.1×10^{-4}
Working pressure (Pa)	5.0×10^{-1}	4.3×10^{-1}	5.5×10^{-1}
Argon flow (sccm)	75	50	50
Oxygen flow (sccm)	2.5	0	0
Deposition time (s)	120	120	120

2.2.2. Deposition and poling of the P(VDF-TrFE) films

P(VDF-TrFE) was dissolved in DMF with a copolymer volume fraction of 15 % by means of a magnetic stirrer (*Agimatic-E*). The vessel containing the mixture was sealed with parafilm to avoid solvent evaporation. In the first 15 min a slight warming of 30 ºC was performed to accelerate the copolymer dissolution and avoid the formation of agglomerates. The mixture was maintained under stirring at room temperature over 2h to obtain a transparent and homogenous solution. After that, approximately 0.6 mL of the P(VDF-TrFE)/DMF solution was deposited on each substrate (pure glass substrate and glass substrates previously coated with TCO-based electrodes) by spin-coating at a rotational velocity, acceleration and time of 1000 rpm, 500 rpm.s^{-1} and 30 s, respectively, and immediately submitted to a thermal treatment of 70 ºC during 30 min by means of a hot-plate (Präzitherm PZ23-2). This procedure allows obtaining P(VDF-TrFE) films with a flat and dense structure, high transparency in the visible spectral range, and homogenous and reproducible thickness of 25 μm. Nevertheless, other thicknesses[40] as well as other PVDF-based polymers films[11, 12] can also be obtained using the same technique. Half of

the prepared samples were poled using a home-made corona chamber to maximize the piezoelectric response of the P(VDF-TFE) films, which is an essential requirement for sensors and actuators applications[9]. The applied voltage and current were 12.5 kV and 20 μA, respectively, with a distance of 2 cm between the sample and the tip. The samples were subjected to the electrical field during 30 min at a poling temperature of 80 ºC and subsequently cooled down to room temperature under electrical field. These parameters were used according to previous studies to maximize the piezoelectric response and guarantee a high optical transparency in the visible spectral range[40, 41].

2.2.3. Deposition of the top TCO-based electrodes

The deposition of the top electrode was performed on the samples that demonstrated better adhesion between the P(VDF-TrFE) films and the lower electrode, which corresponds to the AZO, as will be presented and discussed later in section 3. The deposition procedure was carried out using the same method described in section 2.2.1. Together with optical transparency in the visible spectral range and low resistivity, a preponderant factor when depositing the top electrode is to ensure the integrity of the P(VDF-TrFE) films and their piezoelectric response through deposition at low temperature. Therefore, the top AZO electrode was deposited according to the parameters described in Table 2. The main difference between this procedure and the used one to deposit the bottom AZO electrode comes from the fact that the thin films are deposited in rotation. The rotational velocity was 20 rpm and the deposition time was subdivided in three phases of 300 s spaced from 600 s. Moreover, the substrate bias was reduced to 0V. These process adjustments avoid the overheating of the P(VDF-TrFE) film, which otherwise could compromise the suitable piezoelectric response of the films[39].

Table 2: Deposition parameters for the deposition of top AZO electrode by magnetron sputtering.

Deposition parameters	AZO
Target current density (mA/cm^2)	2.6
Substrate bias (V)	0
Base pressure (Pa)	1.7×10^{-4}
Working pressure (Pa)	4.7×10^{-1}
Argon flow (sccm)	60
Oxygen flow (sccm)	0
Deposition time (s)	300×3
Substrate holder rotation (rpm)	20

2.3. Characterization techniques and procedures

The topography of the TCO's thin films were obtained by atomic force microscopy (AFM) using a multimode platform controlled by a *Nanoscope III*, both from *Veeco*, in the intermittent contact mode. A 5×5 μm^2 area was covered by a silicon tip (resonance frequency of 46-76 kHz, spring contact of 1.2-6.4 N.m^{-1}), purchased from *AppNano*. The contact angles were measured using a *Data Physic OCA20* equipment and ultrapure water was used as test liquid. Water droplets with a volume of 3 μL were placed on the surface of the TCOs thin films. Six measurements were performed in each sample, whereby the contact angle is presented as the mean and standard deviation. In turn, the sheet resistances of the TCO's thin films were measured using a Four Point Probe System composed with probes spaced by 2 mm connected to a *current source DC 9818* from *Time Electronics* and a *2182 nanovoltmeter* from *Keithley*. In order to obtain the electrical resistivity, a correction factor 4.2357 was used (according to a rectangular area of 24×40 mm^2 and thickness lower than 100 nm)[42]. Five measurements were performed at different points of each sample for studying its uniformity. The adhesion between P(VDF-TrFE) films and the bottom TCO electrodes was evaluated based on the ASTM D3359-

97 standard, method B. For coatings up to 50 µm thick, which is the case, a network pattern with 11 cuts spaced 1 mm was designed on the P(VDF-TrFE) films deposited on the TCO substrates by means of a scalpel. An adhesive tape (*Tesa Extra Power Universal* from *Blister*) was then applied to the network pattern and then removed using a universal mechanical test equipment *AG-IS* from *Shimadzu* with a load cell of 50 N, schematically represented in Figure 2. The adhesive tape removal rate was 5 $mm.min^{-1}$. According to the standard, the film/substrate adhesion is evaluated by the percentage of the P(VDF-TrFE) film removed area by the adhesive tape.

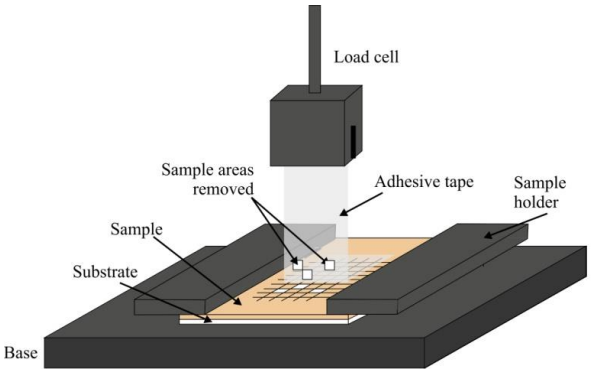

Classification	5	4	3	2	1	0
% of area removed	0 %	< 5 %	5-15 %	15-35 %	35-65%	> 65 %

Figure 2: Schematic representation of the adhesion test based on the ASTM D3359-97 standard, with the respective classification. Adapted from[43].

The optical transmittance of the samples in the visible spectral range was measured using a spectrophotometer *Shimadzu UV-3101PC*. To remove the contribution of the glass substrate and obtain the transmittance spectra of each layer constituting the piezoelectric transducer, the glass substrate was used as reference during the measurements. Finally, the piezoelectric response of the P(VDF-TFE) film was measured with a *d_{33}-meter APC YE2730A*.

3. Results and discussion

The topography and roughness of the bottom TCO's thin films were obtained by AFM. The glass substrates exhibit roughness R_a and R_q of 0.90 nm and 0.95 nm (result not show), respectively. In turn, the ITO (Figure 3(a)), AZO (Figure 3(b)) and GZO (Figure 3(c)) thin films show R_a values of 4.0, 3.9 and 3.6 nm and R_q values of 5.1, 5.2 and 6.2, respectively. Despite their similarity, these measurements do not give a true picture of the real surface profile. In fact, as can be observed on the AFM images, the ITO and AZO's thin films seem to exhibit topographies with uniform peaks, both in size and quantity, being more evident for the AZO samples. In turn, the GZO's thin films present a much lower number of peaks, some of them wider. These small variations in surface topography do not demonstrate a clear and evident effect on the transmittance of the samples in the visible spectral range (Figure 3(d)) and in the contact angle measurements (Figure 3(e)). All of them are characterized by optical transmittances higher than 75% in the entire spectrum. Nevertheless, ITO and GZO optical transmittances decrease when approaching the UV zone, especially for the ITO samples. In turn, the AZO spectrum is more stable, decreasing slightly in the center of the visible spectral range but ensuring a transmittance higher than 85 % throughout the visible range. Regarding Figure 3(e), the results demonstrates that the contact angle behavior is similar for the different TCO's thin films, decreasing over time to a value from which it tends to stabilize. The contact angle generally depends on the deposition process of the water drop on the sample surface. A drop gently deposited on the surface of a substrate spreads continuously until the sum of the forces involved equal zero. The larger the roughness of the film surface, the larger the decrease of the contact angle[44, 45]. Since TCO's thin films exhibit fairly similar roughness, as discussed previously, the same occurs with the decrease of the contact angle. Nevertheless, the ITO's thin films present a slightly higher contact angle (78º±6º at time

0 min to 20º±3º after 60 min) than the AZO (67º±4º at time 0 min to 7º±3º after 60 min) and GZO (65º±5º at time 0 min to 5º±3º after 60 min) thin films, which can be explained by the lower intermolecular interaction between the surface of the sample and the water droplet that overlaps the roughness effects. Consequently, the adhesion of the P(VDF-TrFE) film to the AZO and GZO substrates is expected to be superior to the ITO substrates, since a lower contact angle is associated with a higher hydrophilicity that, in turn, favors adhesion[46, 47].

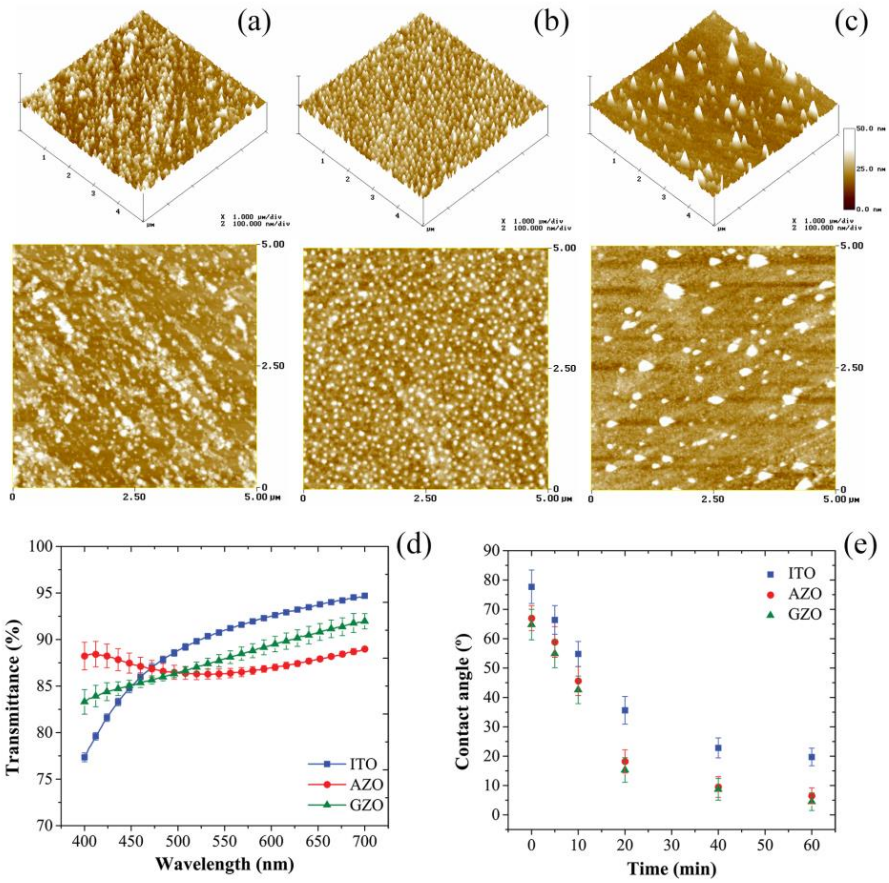

Figure 3: AFM images of the TCO's thin films deposited on the glass substrates (a) ITO, (b) AZO and (c) GZO; (d) Optical transmittance of the TCO's thin films across the visible spectral range; (e) Contact angles of the TCO's thin films measured over 60 min.

As previously indicated, the sheet resistances of the TCO's thin films were measured using a Four Point Probe System. The obtained electrical resistivities demonstrate very

similar values of $(4.1\pm1.7)\times10^{-3}$ Ω.cm, $(3.3\pm0.7)\times10^{-3}$ Ω.cm and $(3.5\pm0.8)\times10^{-3}$ Ω.cm for ITO, AZO and GZO's thin films, respectively. However, AZO and GZO's thin films show relatively lower standard deviations than ITO thin films, proving to be more uniform, with AZO's thin films showing the best results. Moreover, AZO was deposited using the target with bigger area, what results in a greater area of uniformity, in terms of thickness.

Although the optical transmittance spectra and electrical resistivity of the ITO and GZO's thins films demonstrate not to be so good than some published studies [48-50], the same does not happen with the AZO films that exhibit comparable properties with the literature[51, 52]. Further optimization procedures can lead to further improvements of both optical transparency and electrical conductivity[35, 53]. In fact, the resistivity tends to decrease with increasing target current and substrate bias voltage up to a certain optimized value. These two parameters control the kinetic energy of the charged particles, which are responsible for raising the temperature of the substrate. The latter promotes a better organization and packing of the atoms, which is turn allows the production of denser films with fewer defects[54, 55]. Therefore, the heating of the substrate is favorable not only to the reduction of the resistivity, but also to the TCO's thin films roughness reduction, which translates into an increase in the optical transmittance. Excessive energy to the growing film may, however, create defects that lead to an increase of residual stresses. On the other hand, an increase of the time deposition allows obtaining thicker films and with larger crystallinity[56], since the film tends to minimize its surface energy during the growth[57, 58]. In addition, other parameters such as argon flow and oxygen flow may also affect these properties[35, 59]. Nevertheless, the used deposition parameters were optimized to guarantee good properties of the TCO's thin films maintaining a residual increase of the temperature

substrate, which otherwise may jeopardize the integrity of the P(VDF-TrFE) films and its piezoelectric response, in particular during the deposition of the top electrode.

The adhesion tests were performed on the P(VDF-TrFE) films deposited by spin-coating on glass, ITO, AZO and GZO substrates, before and after poling by corona discharge. The samples were previously prepared following the method B of the ASTM D3359-97 standard described in section 2.3. Figure 4(a) illustrates the force exerted by the load cell of the universal mechanical test equipment to remove the adhesive tape attached to the P(VDF-TrFE) film cut into a network of 121 squares of 1 mm^2 area. The number of squares of P(VDF-TrFE) removed during the process is shown in Figure 4(b).

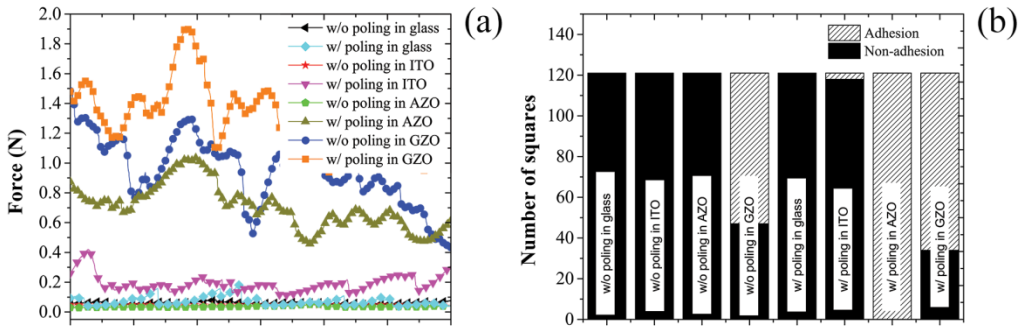

Figure 4: (a) Strength exerted by the load cell of 50 N to remove the adhesive tape applied to the network pattern of the piezoelectric film deposited by spin-coating in the different substrates; (b) Number of squares removed during the process of extracting the adhesive tape. w/o poling mean that the P(VDF-TrFE) films were not poled, while w/ poling means that the P(VDF-TrFE) films were previously poled.

Figure 4 demonstrates that P(VDF-TrFE) films show a poor adhesion to ITO. Almost all squares of non-poled (100 %) and poled P(VDF-TrFE) (98 %) films were removed with a force lower than 0.4 N, exhibiting a behaviour similar to the glass substrate. Therefore, according to the standard presented above, all these samples have a classification of 0. Regarding the samples of P(VDF-TrFE) in GZO substrates, the number of squares removed was 47 (39 %) in the case of the non-poled P(VDF-TrFE) and 34 (28 %) for the

poled P(VDF-TrFE), which corresponds to a classification 1 and 2, respectively. Although the forces exerted to remove the adhesion tape are the highest, the classification obtained indicates a non-suitable adhesion. Moreover, a visual inspection of the squares removed showed traces of GZO, indicating that the GZO's thin films have a week adhesion to the glass substrates. Finally, while the non-poled P(VDF-TrFE) films deposited on AZO substrates show a poor adhesion with a classification of 0 (100 % removed), the poled films remain perfectly adhered to the AZO substrates and therefore feature a maximum rating of 5 (0 % removed). This last result indicates that the adhesion between adhesive tape and poled P(VDF-TrFE) films is inferior to the adhesion of poled films to AZO substrates. Comparing the results of non-poled and poled P(VDF-TrFE) films, it is corroborated that the poling process improves the adhesion between the copolymer film and all substrates tested, including glass, which can be explained by the larger interaction related to the surface charge of the poled copolymer[60]. Therefore, the poling process not just maximizes the piezoelectric response of the P(VDF-TrFE) films but also guarantees their applicability as piezoelectric transducer by ensuring a proper adhesion between the poled P(VDF-TrFE) film and its bottom AZO electrode.

To work as transducer, electrodes must be typically placed on both surfaces of poled P(VDF-TrFE) films, as described in section 2.2.3. The properties of each layer, including the electrical resistivity of the bottom and top AZO electrodes, the piezoelectric coefficient of the poled P(VDF-TrFE) films, the transmittance of each layer and the final properties of the piezoelectric transducer with both electrodes are shown in Table 3.

Table 3: Properties of the transparent piezoelectric P(VDF-TrFE) transducer.

Sample/ Parameter	Resistivity (Ω.cm)	Piezoelectric coefficient $\|d_{33}\|$ ($pC.N^{-1}$)	Transmittance in the visible light spectrum (%)
Bottom AZO electrode	$(3.3\pm0.7)\times10^{-3}$	-	>85
Top AZO electrode	$(11.3\pm 1.7)\times10^{-3}$	-	>80
Poled P(VDF-TrFE) film	-	34	> 85
Piezoelectric P(VDF-TrFE) transducer w/ AZO electrodes	-	34	>75
Piezoelectric P(VDF-TrFE) transducer w/ AZO electrodes and glass substrate	-	34	>62

The top electrode features a slightly higher resistivity and lower transmittance comparatively to the bottom electrode, which is justified by the adjustment of the sputtering parameters to guarantee a low deposition temperature and therefore the integrity of the P(VDF-TrFE) piezoelectricity. In fact, the deposition of the top electrode did not affect the piezoelectric coefficient $|d_{33}|$ that maintain a value of 34 $pC.N^{-1}$ (the d_{33} piezoelectric coefficient is negative). Moreover, it should be noted that the deposition of the P(VDF-TrFE) directly on the bottom AZO electrode allows a more efficient electrical poling due to the higher homogeneity of the electrical potential. Regarding the optical transmittance of the piezoelectric P(VDF-TrFE) transducer with AZO electrodes, a maximum value of 85 % that decreases when approaching the UV zone, reaching 75 % at 400 nm, is obtained. This result confirms the successful optimization of the deposition parameters of the piezoelectric P(VDF-TrFE) film as well as the AZO electrodes to obtain a high optical transmittance in the visible spectral range. Nevertheless, the glass used in this work as substrate for the deposition of the various layers that constitute the piezoelectric transducer leads to a decrease in the transmittance of approximately 13 % across the spectrum. It should be noted that although the deposition parameters of P(VDF-TrFE) films by spin-coating were adjusted in order to obtain a thickness of 25 μm, other

thicknesses as well as other PVDF based polymers can be also be processed[11, 12, 40], as previously indicated. The optimized P(VDF-TrFE) transducer with AZO electrodes certainly has a strong potential for applications. Its high piezoelectric properties and light transmission makes it a good candidate for light sensitive applications, like haptic technology[61, 62], optoacoustic systems for biomedical applications[20], photovoltaic cells[29, 63], LEDs[33, 34] and LCDs [30], representing a good alternative to transducers with ITO electrodes.

4. Conclusions

Piezoelectric P(VDF-TrFE) transducers with high transmittance in the visible spectral range, with high piezoelectric coefficient and with strong adhesion between the piezoelectric film and the electrodes were fabricated using different deposition techniques. Various TCOs electrodes, namely ITO, AZO and GZO, were studied and deposited by magnetron sputtering in glass substrates, while P(VDF-TrFE) films were deposited by spin-coating. All layers constituting the piezoelectric transducer were properly processed and characterized. The results demonstrated that P(VDF-TrFE) films show a strong adhesion to AZO substrates after electrical poling, which indicate that this process not just maximize the piezoelectric response of the copolymer films but also guarantees the proper adhesion between these layers. The optimized P(VDF-TrFE) transducer with AZO electrodes shows an optical transmittance higher than 75 % in the visible spectral range and a piezoelectric coefficient $|d_{33}|$ of 34 $pC.N^{-1}$. This result confirms the successful optimization of the deposition parameters of each layer allowing the deposition of the piezoelectric transducer on any substrate without using any further adhesion layer. Further, it is shown that the integrity and piezoelectric response of the

copolymer film is guaranteed after the deposition of the top AZO electrode at low temperature.

Acknowledgments

The authors thank the FCT - Fundação para a Ciência e Tecnologia - for financial support under framework of the Strategic Funding UID/FIS/04650/2013, project PTDC/EEI-SII/5582/2014 and project UID/EEA/04436/2013 by FEDER funds through the COMPETE 2020 – Programa Operacional Competitividade e Internacionalização (POCI) with the reference project POCI-01-0145-FEDER-006941. Funds provided by FCT in the framework of EuroNanoMed 2016 call, Project LungChek ENMed/0049/2016 are also gratefully acknowledged. VFC also thanks the FCT for the grant SFRH/BPD/98109/2013. Finally, the authors acknowledge funding by the Spanish Ministry of Economy and Competitiveness (MINECO) through the project MAT2016-76039-C4-3-R (AEI/FEDER, UE) and from the Basque Government Industry Department under the ELKARTEK and HAZITEK programs.

References

1. B. Adhikari and S. Majumdar, Prog. Polym. Sci. **29** (7), 699-766 (2004).
2. V. F. Cardoso, C. Ribeiro and S. Lanceros-Mendez, in *Bioinspired Materials for Medical Applications* (2016), pp. 69-99.
3. S. Guragain, B. P. Bastakoti, V. Malgras, K. Nakashima and Y. Yamauchi, Chem.-Eur. J. **21** (38), 13164-13174 (2015).
4. R. Bogue, Assem. Autom. **34** (1), 16-22 (2014).
5. K. S. Ramadan, D. Sameoto and S. Evoy, Smart Materials and Structures **23** (3) (2014).
6. A. H. Rajabi, M. Jaffe and T. L. Arinzeh, Acta Biomaterialia **24**, 12-23 (2015).
7. R. A. P. Altafim, X. Qiu, W. Wirges, R. Gerhard, R. A. C. Altafim, H. C. Basso, W. Jenninger and J. Wagner, Journal of Applied Physics **106** (1) (2009).
8. N. Wu, S. Chen, S. Lin, W. Li, Z. Xu, F. Yuan, L. Huang, B. Hu and J. Zhou, Journal of Materials Chemistry A **6** (12), 5065-5070 (2018).
9. P. Martins, A. C. Lopes and S. Lanceros-Mendez, Prog. Polym. Sci. **39** (4), 683-706 (2014).
10. J. Nunes-Pereira, P. Martins, V. F. Cardoso, C. M. Costa and S. Lanceros-Mendez, Materials & Design **104**, 183-189 (2016).

11. V. F. Cardoso, G. Minas and S. Lanceros-Méndez, Sensors and Actuators, A: Physical **192**, 76-80 (2013).
12. V. F. Cardoso, G. Minas, C. M. Costa, C. J. Tavares and S. Lanceros-Mendez, Smart Materials & Structures **20** (8), 087002 (2011).
13. X. Yu, R. Rajamani, K. A. Stelson and T. Cui, Sensor Actuat a-Phys **132** (2), 626-631 (2006).
14. D. S. Hecht, D. Thomas, L. B. Hu, C. Ladous, T. Lam, Y. Park, G. Irvin and P. Drzaic, J Soc Inf Display **17** (11), 941-946 (2009).
15. G. W. J. Brodie, Y. Q. Qiu, S. Cochran, G. C. Spalding and M. P. MacDonald, Ieee T Ultrason Ferr **61** (3), 389-391 (2014).
16. D. Sette, S. Girod, N. Godard, N. Adjeroud, J. B. Chemin, R. Leturcq and E. Defay, Proc Ieee Micr Elect, 793-796 (2017).
17. J. Li, Gaofenzi Cailiao Kexue Yu Gongcheng/Polymeric Materials Science and Engineering **29** (11), 173-176+182 (2013).
18. Y. Wu, Z. Yi, Z. Ge, F. Du and Y. Zhang, Cailiao Daobao/Materials Review **31** (4), 26-31 (2017).
19. O. Edynoor, A. R. M. Warikh, T. Moriga, K. Murai and M. E. A. Manaf, Rev. Adv. Mater. Sci. **49** (2), 150-157 (2017).
20. J. J. Niederhauser, M. Jaeger, M. Hejazi, H. Keppner and M. Frenz, Opt Commun **253** (4-6), 401-406 (2005).
21. J. W. Gao, K. Kempa, M. Giersig, E. M. Akinoglu, B. Han and R. P. Li, Advances in Physics **65** (6), 553-617 (2016).
22. T. Minami, in *Oxide Semiconductors*, edited by B. G. Svensson, S. J. Pearton and C. Jagadish (2013), Vol. 88, pp. 159-200.
23. A. Illiberi, P. Poodt, P. J. Bolt and F. Roozeboom, Chemical Vapor Deposition **20** (7-9), 234-242 (2014).
24. P. C. Mondal, V. Singh and M. Zharnikov, Accounts Chem. Res. **50** (9), 2128-2138 (2017).
25. B. Vonhoeren, S. Dalgleish, L. Hu, M. M. Matsushita, K. Awaga and B. J. Ravoo, ACS Applied Materials and Interfaces **7** (13), 7049-7053 (2015).
26. A. Kimoto and T. Kitajima, Measurement Science and Technology **21** (3) (2010).
27. R. B. H. Tahar, T. Ban, Y. Ohya and Y. Takahashi, Journal of Applied Physics **83** (5), 2631-2645 (1998).
28. C. G. Granqvist and A. Hultaker, Thin Solid Films **411** (1), 1-5 (2002).
29. P. Dai, J. Y. Lu, M. Tan, Q. S. Wang, Y. Y. Wu, L. Ji, L. F. Bian, S. L. Lu and H. Yang, Chinese Phys B **26** (3) (2017).
30. M. Sawada, M. Higuchi, S. Kondo and H. Saka, Jpn J Appl Phys 1 **40** (5A), 3332-3336 (2001).
31. D. S. Hecht, L. B. Hu and G. Irvin, Adv Mater **23** (13), 1482-1513 (2011).
32. C. H. Hong, J. H. Shin, B. K. Ju, K. H. Kim, N. M. Park, B. S. Kim and W. S. Cheong, J Nanosci Nanotechno **13** (11), 7756-7759 (2013).
33. K. Molnar, T. Mohacsy, P. Varga, E. Vazsonyi and I. Barsony, J Lumin **80** (1-4), 91-97 (1998).
34. W. Yan, W. Guo, B. Cui, W. Gao, F. Yin and D. Cui, presented at the Remote Sensing, Environment and Transportation Engineering (RSETE), 2011 International Conference on, 2011 (unpublished).
35. T. Minami, Thin Solid Films **516** (17), 5822-5828 (2008).
36. E. M. Bomhard, Environmental Toxicology and Pharmacology **45**, 282-294 (2016).
37. Y. Zeng, Z. Q. Fang, H. L. Ning, F. Zhu, X. Z. Liu, R. Q. Tao, S. B. Hu, R. H. Yao, Z. C. Li, M. Xu, L. Wang, L. F. Lan and J. B. Peng, Molecular Crystals and Liquid Crystals **644** (1), 190-196 (2017).
38. R. G. Gordon, Mrs Bulletin **25** (8), 52-57 (2000).
39. M. P. Silva, C. M. Costa, V. Sencadas, A. J. Paleo and S. Lanceros-Méndez, Journal of Polymer Research **18** (6), 1451-1457 (2011).

40. V. F. Cardoso, C. M. Costa, G. Minas and S. Lanceros-Mendez, Smart Materials and Structures **21** (8), 085020 (2012).
41. V. F. Cardoso, T. Knoll, T. Velten, L. Rebouta, P. M. Mendes, S. Lanceros-Méndez and G. Minas, RSC Adv. **4** (9), 4292-4300 (2014).
42. F. M. Smits, Bell System Technical Journal **37** (3), 711-718 (1958).
43. N. A. Trujillo, R. A. Oldinski, H. Y. Ma, J. D. Bryers, J. D. Williams and K. C. Popat, Mater. Sci. Eng. C-Mater. Biol. Appl. **32** (8), 2135-2144 (2012).
44. D. Quere, in *Annual Review of Materials Research* (2008), Vol. 38, pp. 71-99.
45. Y. J. Lim, Y. Oshida, C. J. Andres and M. T. Barco, International Journal of Oral & Maxillofacial Implants **16** (3), 333-342 (2001).
46. L. Ponsonnet, K. Reybier, N. Jaffrezic, V. Comte, C. Lagneau, M. Lissac and C. Martelet, Materials Science & Engineering C-Biomimetic and Supramolecular Systems **23** (4), 551-560 (2003).
47. K. Mittal, *Advances in Contact Angle, Wettability and Adhesion*. (2015).
48. D. H. Kim, M. R. Park and G. H. Lee, Surf. Coat. Technol. **201** (3-4), 927-931 (2006).
49. S. K. Park, J. I. Han, W. K. Kim and M. G. Kwak, Thin Solid Films **397** (1-2), 49-55 (2001).
50. K. Nagamoto, K. Kato, S. Naganawa, T. Kondo, Y. Sato, H. Makino, N. Yamamoto and T. Yamamoto, Thin Solid Films **520** (5), 1411-1415 (2011).
51. J. Y. Kao, C. Y. Hsu, G. C. Chen and D. C. Wen, J. Mater. Sci.-Mater. Electron. **23** (7), 1352-1360 (2012).
52. X. J. Wang, X. B. Zeng, D. Q. Huang, X. Zhang and Q. Li, J. Mater. Sci.-Mater. Electron. **23** (8), 1580-1586 (2012).
53. H. Hosono, D. C. Paine and D. Ginley, *Handbook of Transparent Conductors*. (Springer US, 2011).
54. T. Tohsophon and N. Sirikulrat, Solar Energy Materials and Solar Cells **90** (18-19), 3444-3448 (2006).
55. F. Ruske, A. Pflug, V. Sittinger, W. Werner, B. Szyszka and D. J. Christie, Thin Solid Films **516** (14), 4472-4477 (2008).
56. E. Fortunato, A. Goncalves, V. Assuncao, A. Marques, H. Aguas, L. Pereira, I. Ferreira and R. Martins, Thin Solid Films **442** (1-2), 121-126 (2003).
57. K. H. Kim, R. A. Wibowo and B. Munir, Materials Letters **60** (15), 1931-1935 (2006).
58. S. K. Jung, S. H. Lee, Y. S. Lee, S. M. Lee, L. S. Park and S. H. Sohn, Molecular Crystals and Liquid Crystals **499**, 638-646 (2009).
59. M. Chen, Z. L. Pei, C. Sun, J. Gong, R. F. Huang and L. S. Wen, Materials Science and Engineering B-Solid State Materials for Advanced Technology **85** (2-3), 212-217 (2001).
60. J. S. Nunes, V. Sencadas, A. Wu, P. M. Vilarinho and S. Lanceros-Mendez, in *Advanced Materials Forum Iii, Pts 1 and 2*, edited by P. M. Vilarinho (2006), Vol. 514-516, pp. 915-919.
61. Y. Xin, H. Y. Tian, C. Guo, X. Li, H. S. Sun, P. Y. Wang, J. Lin, S. H. Wang and C. Wang, Ferroelectrics **504** (1), 31-45 (2016).
62. A. Akther, A. Katy, H. C. Kim and J. Kim, Nanosensors, Biosensors, and Info-Tech Sensors and Systems 2016 **9802** (2016).
63. H. Y. Liu, V. Avrutin, N. Izyumskaya, U. Ozgur and H. Morkoc, Superlattice Microst **48** (5), 458-484 (2010).